Asymptotic and numerical solutions of the initial value problem in rotating planetary fluid cores

X. Liao[1] and K. Zhang[2]

[1]*Shanghai Astronomical Observatory, Chinese Academy of Sciences, Shanghai* 200030*, PR China*
[2]*Center for Geophysical and Astrophysical Fluid Dynamics and Department of Mathematical Sciences, University of Exeter,* EX4 4QE, *UK.*
E-mail: kzhang@ex.ac.uk

SUMMARY

An initial state of fluid motion in planetary cores or atmospheres, excited, for example, by the giant impact of an asteroid or an earthquake and then damped by viscous dissipation, decays towards the state of rigid-body rotation. The process of how the initial state approaches the final state, the initial value problem, is investigated both analytically and numerically for rotating fluid spheres. We derive an explicit asymptotic expression for the time-dependent solution of the initial value problem valid for an asymptotically small Ekman number E. We also perform a fully numerical analysis to simulate time-dependent solutions of the initial value problem for a small value of E. Comparison between the asymptotic solution and the corresponding numerical simulation shows a satisfactory quantitative agreement. For the purpose of illustrating why spherical geometry represents an intricate and exceptional case, we also briefly discuss the initial value problem in a rotating fluid channel. Geophysical and planetary physical implications of the result are also discussed.

Key words: Earth rotation variations; Dynamo: theories and simulations; Core, outer core and inner core.

1 INTRODUCTION

Fluid motion encountered in geophysical and planetary systems can be divided into two different categories: unforced problems and continuously forced problems. The forced problem includes fluid motion continuously driven by convective instabilities taking place in planetary fluid cores (Jones *et al.* 2000; Aubert *et al.* 2001; Dormy *et al.* 2004) or by planetary precession (Tilgner & Busse 2001) or by planetary libration (Noir *et al.* 2008). The unforced problem is concerned with how a given initial state of fluid motion is damped by viscous dissipation and then decays towards a state of rigid-body rotation. In the fluid dynamics literature, the unforced problem is usually referred to as the initial value problem (Greenspan 1968).

The initial value problem in rapidly rotating spherical systems is of direct relevance to many geophysical and planetary physical problems. This is because there are sudden variations taking place in the geophysical and planetary physical systems where the subsequent fluid motion can be described by a solution of the initial value problem. For example, how an initial state of fluid motion excited by an earthquake (Aldridge & Lumb 1987) or tide (Kerswell 1994) or planet-comet/asteroid clash such as Comet Shoemaker-Levy 9 on Jovian atmosphere (Kerr 1994) is damped by viscous dissipation and then decays towards a state of rigid-body rotation. In a recent study, Arkani-Hamed *et al.* (2008) propose a causative relationship between the giant impacts of asteroids and the Martian core dynamo. Length-of-day variations of the Earth on a decadal timescale, which is attributed to the exchange of angular momentum

between the solid mantle and fluid core (Jault *et al.* 1988; Holme 1998; Holme & de Viron 2005), may also excite fluid motion in the Earth's fluid core. Recent observations show that Titan's spin is non-synchronous, indicating angular momentum exchange between Titan's surface and the atmosphere over seasonal timescales (van Hoolst *et al.* 2009). An asymptotic time-dependent solution of the initial value problem helps us understand the relevant temporal change of the amplitude and structure of such excited flows.

It is hence highly desirable, in the interest of geophysical and planetary physical context, that an asymptotic analytical expression valid for an asymptotically small Ekman number, which is fairly straightforward to compute, can be derived to describe how an arbitrary initial state in rotating spherical fluid systems is damped by viscous dissipation and changes towards a different state. Although the initial value problem in rotating spherical systems represents an important classical geophysical problem various aspects of which have been studied (Greenspan 1968; Rieutord & Valdettaro 1997; Schmitt 2006) [for example, the viscous decay factors of several spherical inertial modes were carefully studied, (Greenspan 1968; Hollerbach & Kerswell 1995; Liao & Zhang 2008)], an explicit asymptotic time-dependent solution of the initial value problem in rapidly rotating spheres has not been obtained and validated. This study revisits this classical geophysical problem by deriving the first explicit expression of the asymptotic time-dependent solution of the initial value problem in rotating fluid spheres valid for an asymptotically small Ekman number E and by validating the asymptotic solution with the numerical simulation of the same problem at a

sufficiently small E. The asymptotic formulae presented in this paper are complicated but fairly straightforward to compute and are applicable to many geophysical problems that are concerned with how an original state is reconciled with a sudden change by adjusting its fluid motion.

An asymptotic description of the initial value problem for general rapidly rotating fluid systems was outlined and formulated by Greenspan (1968) several decades ago. His asymptotic theory for the initial-value problem is based on expansions in half powers of the Ekman number E, where E is assumed to be asymptotically small. By assuming that the initial state varies only slightly from rigid-body rotation, an essential analysis in the asymptotic theory is to determine the viscous decay factor, d_m, of an inertial mode, which is given by, for example, eq. (2.9.12) in Greenspan's monograph (1968),

$$d_m = \frac{\int_S p_m^* F_m \, dS}{\int_V \mathbf{u}_m^* \cdot \mathbf{u}_m \, dV}, \tag{1}$$

where $\mathbf{u}_m$ is the velocity of an inviscid inertial mode with $\mathbf{u}_m^*$ being its complex conjugate, p_m^* denotes the complex conjugate of the pressure for the inertial mode, F_m is the mass flux from the Ekman boundary layer, $\int_S$ represents a surface integral over the bounding surface of a container and $\int_V$ denotes a volume integral over the container. In a recent study (Zhang & Liao 2008) on the initial value problem in rotating circular cylinders, however, it was revealed that the effects of spatial and temporal non-uniformities obscure the form of the expansion even in the first viscous corrective terms and, consequently, $E^{1/2}$ cannot be taken as an expansion parameter in the process of deriving an accurate asymptotic solution. It was also shown that a satisfactory quantitative agreement between the asymptotic analysis that is based on (1) and the numerical analysis cannot be achieved for rotating cylinders. Zhang & Liao (2008) then suggested the modified asymptotic formula

$$d_m = \frac{\int_S p_m^* F_m \, dS + E \int_V \mathbf{u}_m^* \cdot \nabla^2 \mathbf{u}_m \, dV}{\int_V \mathbf{u}_m^* \cdot \mathbf{u}_m \, dV}. \tag{2}$$

In other words, the internal viscous dissipation, given by $E \int_V \mathbf{u}_m^* \cdot \nabla^2 \mathbf{u}_m \, dV$, cannot generally be neglected. The internal viscous effect is perhaps most clearly illustrated by the initial value problem in a rotating channel because an analytical expression for d_m in close form can be derived. As we shall show in Appendix A,

$$\left| \frac{E \int_V \mathbf{u}_m^* \cdot \nabla^2 \mathbf{u}_m \, dV}{\int_S p_0^* F_m \, dS} \right| \geq O(1) \tag{3}$$

for an arbitrarily small Ekman number E as long as the vertical wavenumber of an inertial wave $n \geq O(E^{-1/6})$. It follows that a satisfactory quantitative agreement between the analytical expression based on expansions in half powers of E and the fully numerical analysis is not expected for a channel if the formula (1), which neglects the dominant contribution from the term $E \int_V \mathbf{u}_m^* \cdot \nabla^2 \mathbf{u}_m \, dV$, is adopted, as will be discussed in Appendix A.

An asymptotic solution of the initial value problem for rapidly rotating spheres would be profoundly different. At the root of the difference is the unusual integral property of spherical inertial waves,

$$\int_V \mathbf{u}_m^* \cdot \nabla^2 \mathbf{u}_m \, dV \equiv 0, \tag{4}$$

which was first revealed by Zhang *et al.* (2001). It is because of the unexpected/unusual property (4) that the asymptotic formula (1), which cannot provide a satisfactory asymptotic solution for non-spherical geometries such as cylinders and channels, can lead to a satisfactory quantitative agreement between the asymptotic

and numerical analysis for rotating spheres. However it should be borne in mind that, despite the fact that the property (4) can be mathematically rigorously proved, many questions still remain about its mathematical and physical significance.

Although the general asymptotic ideas for the initial-value problem in rotating fluid spheres were developed several decades ago by Greenspan (1968), the effort to derive an explicit asymptotic solution of the problem was hampered by the absence of explicit inertial wave solutions in spherical geometry. With the availability of explicit analytical solutions for all inertial waves (Zhang *et al.* 2001), which are expressed in terms of double Poincaré polynomials (Zhang & Liao 2004), we are now in the position to derive the explicit asymptotic solution describing how an arbitrary initial state in a fluid sphere with an arbitrarily small Ekman number E is damped by viscous dissipation and then decays towards a state of rigid-body rotation. Since it is experimentally difficult to measure accurately a solution of the initial value problem in rotating spherical systems, the accuracy of an asymptotic solution at an arbitrarily small E can be only validated by full numerical analysis of the problem at a sufficiently small E. In this study, we shall show, by performing direct numerical integrations for the initial value problem in the range $10^{-3} \leq E \leq 10^{-5}$, that a satisfactory agreement between our asymptotic time-dependent solution and the fuller numerics can be achieved.

In what follows we shall begin by presenting the mathematical formulation of the problem in Section 2. The asymptotic analysis of the problem is discussed in Section 3 and the corresponding numerical simulation, as well as its comparison with the asymptotic solution, is presented in Section 4. Possible geophysical applications of the asymptotic solution is discussed in Section 5 while the paper closes in Section 6 with a brief summary and some remarks. The initial value problem in a rotating fluid channel is briefly discussed in Appendix A.

2 MATHEMATICAL FORMULATION OF THE PROBLEM

We consider an incompressible viscous fluid filling a full sphere of radius r_o rotating uniformly with a constant angular velocity $\boldsymbol{\Omega}$. The possible effects of an inner core (Rieutord *et al.* 2002), as well as compressibility (Seyed-Mahmoud *et al.* 2007), are ignored. At a particular time, $t = 0$, a physically acceptable initial condition consisting of a small-Rossby-number fluid motion, $\mathbf{U}_0$, which may be excited by an external event such as an earthquake (Aldridge & Lumb 1987), is imposed within the rotating fluid sphere. The manner in which this initial state approaches the final state of solid-body rotation is described by the following dimensionless equations (Greenspan 1968) in the rotating reference frame

$$\frac{\partial \mathbf{u}}{\partial t} + \mathbf{u} \cdot \nabla \mathbf{u} + 2\hat{\mathbf{z}} \times \mathbf{u} = -\nabla p + E \nabla^2 \mathbf{u}, \tag{5}$$

$$\nabla \cdot \mathbf{u} = 0, \tag{6}$$

subject to the boundary conditions

$$\mathbf{u}(r = 1) = 0 \tag{7}$$

and the initial condition

$$\mathbf{u}(\mathbf{r}, t = 0) = \mathbf{U}_0(\mathbf{r}), \tag{8}$$

where $\hat{\mathbf{z}}$ denotes the unit vector parallel to the axis of rotation Ω, $\mathbf{u}$ is the 3-D velocity field, (u_r, u_θ, u_ϕ), in spherical polar coordinates

(r, θ, ϕ) with the unit vectors $(\hat{\mathbf{r}}, \hat{\boldsymbol{\theta}}, \hat{\boldsymbol{\phi}})$ and with $\theta = 0$ representing the axis of rotation, and p is the reduced pressure. Following Greenspan's general formulation (Greenspan 1968), we shall assume that the amplitude of $\mathbf{U}_0$ is sufficiently small such that the non-linear term $\mathbf{u} \cdot \nabla \mathbf{u}$ can be neglected.

In the dimensionless eqs (5) and (6), the radius of the sphere r_o is employed as the length scale and $|\Omega|^{-1}$ is used as the unit of time. It follows that the problem is simply characterized by one dimensionless parameter, the Ekman number E, defined as

$$E = \frac{\nu}{|\Omega| r_o^2},$$

where ν is kinematic viscosity of the fluid, together with the structure of the initial flow $\mathbf{U}_0$. For applications to planetary fluid systems like the Earth's core, which are usually rapidly rotating, we shall assume that the value of E is extremely small, that is, $E \ll 1$. Without loss of any key physics of the problem, we shall also assume an initial state of the fluid motion, $\mathbf{U}_0$, is non-axisymmetric, involving only a single azimuthal wavenumber.

A time-dependent initial value problem in rapidly rotating fluid spheres with $E \ll 1$ is then defined by partial differential eqs (5) and (6) subject to the conditions (7) and (8). In the first part of our study, we shall derive an asymptotic solution of the initial value problem for an asymptotically small E. In the second part, we shall integrate (5) and (6) numerically to obtain the time-dependent solution of the problem for small values of E.

It is worth mentioning that solutions to the linearized eqs (5) and (6) with the spherically symmetric condition (7) can be divided into two different classes according to their spatial symmetries with respect to the equatorial plane at $\theta = \pi/2$: the equatorially symmetric solutions obeying

$$\left(u_\phi, u_r, u_\theta\right)(r, \theta, \phi) = \left(u_\phi, u_r, -u_\theta\right)(r, \pi - \theta, \phi) \tag{9}$$

and the equatorially antisymmetric solutions whose parity satisfy

$$\left(u_\phi, u_r, u_\theta\right)(r, \theta, \phi) = \left(-u_\phi, -u_r, u_\theta\right)(r, \pi - \theta, \phi). \tag{10}$$

Since both the asymptotic and numerical analyses for the equatorially symmetric and antisymmetric solutions are entirely analogous, we shall focus only on the equatorially symmetric solution of the initial value problem subject to the equatorially symmetric initial condition.

3 ASYMPTOTIC SOLUTION OF THE INITIAL VALUE PROBLEM

Consider time-dependent solutions of the initial value problem in a rapidly rotating sphere over the timescale $O(E^{-1/2})$, where E is arbitrarily small but fixed, subject to any physically acceptable initial condition whose spatial scale is much larger than $O(E^{1/2})$. Since, generally speaking, the effects of spatial and temporal non-uniformities obscure the form of the expansion even in the first viscous corrective terms (Zhang & Liao 2008), we shall not take $E^{1/2}$ as an expansion parameter in the asymptotic solution of the initial value problem. Consequently, the asymptotic expansion of Greenspan (1968) is modified such that the fluid velocity $\mathbf{u}$ and other variables for the initial value problem are expanded in the following manner

$$\mathbf{u} = \mathbf{u}_0 + \tilde{\mathbf{u}}_0 + \mathbf{u}_1,$$

$$\mathbf{p} = p_0 + \tilde{p}_0 + p_1, \tag{11}$$

where $\mathbf{u}_0$ and p_0 denote the leading-order interior solution, $\tilde{\mathbf{u}}_0$ and $\tilde{p}_0$ are the corresponding viscous boundary layer and, $\mathbf{u}_1$ and p_1

represent the small secondary interior solution with

$$|\mathbf{u}_0| = O(|\tilde{\mathbf{u}}_0|) \gg O(|\mathbf{u}_1|).$$

The velocity can be further expressed as

$$\mathbf{u}_0 = \sum_{mnk} A_{mnk} \mathbf{u}_{mnk} \exp\left[(\hat{\imath}\omega_{mnk} + \hat{\imath}\omega_{mnk1} - d_{mnk})t\right],$$

$$\tilde{\mathbf{u}}_0 = \sum_{mnk} A_{mnk} \left(\tilde{\mathbf{u}}_{mnk} + \tilde{\mathbf{u}}_{mnk1}\right),$$

$$\mathbf{u}_1 = \sum_{mnk} \mathbf{u}_{mnk1}, \tag{12}$$

where $\hat{\imath} = \sqrt{-1}$, $\mathbf{u}_{mnk} = O(1)$ represents an inviscid 3-D spherical inertial mode described by the three indices (m, n, k) in relation to the three spatial wavenumbers in the azimuthal, vertical and radial directions, respectively, ω_{mnk} is real, denoting the frequency of the inviscid inertial mode, ω_{mnk1} is the small viscous correction of the inviscid frequency, A_{mnk} is, to leading approximation, given by

$$A_{mnk} = \frac{\int_0^{2\pi}\int_0^{\pi}\int_0^1 \mathbf{u}_{mnk}^* \cdot \mathbf{U}_0 r^2 \sin\theta \, \mathrm{d}r \, \mathrm{d}\theta \, \mathrm{d}\phi}{\int_0^{2\pi}\int_0^{\pi}\int_0^1 |\mathbf{u}_{mnk}|^2 r^2 \sin\theta \, \mathrm{d}r \, \mathrm{d}\theta \, \mathrm{d}\phi}, \tag{13}$$

$\tilde{\mathbf{u}}_{mnk} = O(1)$ is the tangential boundary correction due to the effect of viscosity while $\tilde{\mathbf{u}}_{mnk1}$ represents the small secondary boundary flow including the radial flux, d_{mnk} is real and represents the viscous decay factor of the inertial mode and $\mathbf{u}_{mnk1}$ satisfying $|\mathbf{u}_{mnk1}| \ll |\mathbf{u}_{mnk}|$ denotes the small secondary interior solution. The pressure field can be expanded in a similar way. In comparison to the previously used expansion, for example, eqs (2.5.6) and (2.5.8) in (Greenspan 1968), the modified expansion (11) does not take $E^{1/2}$ as an expansion parameter and, consequently, gives rise to a different asymptotic sequence. We shall also use the half-frequency σ_{mnk} in our asymptotic analysis, that is, $\omega_{mnk} = 2\sigma_{mnk}$, because of the property $|\sigma_{mnk}| < 1$. Moreover, in order to save space in writing down the mathematical expressions, we sometimes do not use the subscript notation if and when no confusion arises.

In an asymptotic solution of the initial value problem, as explained by (Greenspan 1968), there exist three major elements—inviscid inertial waves $\mathbf{u}_{mnk}$, the viscous boundary correction $\tilde{\mathbf{u}}_{mnk}$ and the viscous decay factor d_{mnk}—which can be obtained from three different problems in the asymptotic sequence. After substitution of the expansion (11) into the governing eqs (5) and (6), the first problem in the asymptotic sequence is concerned with the zero-order interior solution of the inviscid motion, governed by the dimensionless equations

$$\hat{\imath}2\sigma_{mnk}\mathbf{u}_{mnk} + 2\hat{\mathbf{z}} \times \mathbf{u}_{mnk} = -\nabla p_{mnk}, \tag{14}$$

$$\nabla \cdot \mathbf{u}_{mnk} = 0, \tag{15}$$

where $\omega_{mnk} = 2\sigma_{mnk}$ and $|\sigma_{mnk}| < 1$, subject to

$$\hat{\mathbf{r}} \cdot \mathbf{u}_{mnk} = 0 \tag{16}$$

on the bounding surface of the sphere. The explicit general analytical solution for the first problem in the asymptotic sequence was found by Zhang *et al.* (2001), which can be conveniently rewritten in spherical polar coordinates. A general expression of the pressure and velocity for all the spherical inertial modes with equatorial symmetry (9) is

$$p_{mnk} = \sum_{i=0}^{k}\sum_{j=0}^{k-i} r^{m+2(i+j)} C_{mkij}\sigma^{2i-1}(1-\sigma^2)^{j-1}$$

$$\times \sin^{m+2j}\theta \cos^{2i}\theta \, \mathrm{e}^{\hat{\imath}(m\phi)}, \tag{17}$$

$$\hat{\mathbf{r}} \cdot \mathbf{u}_{mnk} = -\frac{\tilde{\imath}}{2} \sum_{i=0}^{k} \sum_{j=0}^{k-i} C_{mkij} r^{m+2(i+j)-1} \sigma^{2i-1} (1-\sigma^2)^{j-1}$$
$$\times \sin^{m+2j} \theta \cos^{2i} \theta$$
$$\times \left[\sigma(m + m\sigma + 2j\sigma) - 2i(1-\sigma^2) \right] e^{\tilde{\imath}(m\phi)}, \tag{18}$$

$$\hat{\boldsymbol{\theta}} \cdot \mathbf{u}_{mnk} = -\frac{\tilde{\imath}}{2} \sum_{i=0}^{k} \sum_{j=0}^{k-i} C_{mkij} r^{m+2(i+j)-1} \sigma^{2i-1} (1-\sigma^2)^{j-1}$$
$$\times \left[\sigma(m + m\sigma + 2j\sigma) \cos^2\theta + 2i(1-\sigma^2)\sin^2\theta \right]$$
$$\times \sin^{m+2j-1} \theta \cos^{2i-1} \theta e^{\tilde{\imath}(m\phi)}, \tag{19}$$

$$\hat{\boldsymbol{\phi}} \cdot \mathbf{u}_{mnk} = \frac{1}{2} \sum_{i=0}^{k} \sum_{j=0}^{k-i} C_{mkij} r^{m+2(i+j)-1} \sin^{m+2j-1} \theta \cos^{2i} \theta$$
$$\times \left[\sigma^{2i} (1-\sigma^2)^{j-1} (m + m\sigma + 2j) \right] e^{\tilde{\imath}(m\phi)}, \tag{20}$$

where C_{mkij} is defined as

$$C_{mkij} = \frac{(-1)^{i+j} [2(k+i+j+m)-1]!!}{2^{j+1}(2i-1)!!(k-i-j)!i!j!(m+j)!},$$

along with

$$(2i-1)!! = (2i-1)(2i-3)\ldots\ldots(3)(1), \quad (-1)!! = 1, \quad (0)! = 1.$$

Here the half frequencies, σ, for the equatorially symmetric modes are the solutions of

$$\sum_{j=0}^{k-1} \frac{(-1)^{j+k}[2(2k+m-j)]!}{j!(2k+m-j)![2(k-j)]!}$$
$$\times [(m+2k-2j)\sigma - 2(k-j)] \sigma^{2(k-j)-1}$$
$$+ \frac{m[2(k+m)]!}{k!(k+m)!} = 0, \tag{21}$$

where $k = 1, 2, 3 \ldots$ and m denotes an azimuthal wavenumber. There exist $2k$ different solutions to (21), which can be arranged, with the aid of subscript notation, according to the size of σ, for example,

$$0 < |\sigma_{m1k}| < |\sigma_{m2k}| < |\sigma_{m3k}|, \ldots, < |\sigma_{mnk}| < \ldots,$$

where σ_{mnk} denotes the nth smallest root to (21) for given m and k. Furthermore, (18)–(20) can be conveniently cast in the form,

$$\mathbf{u}_{mnk} = [\tilde{\imath}\hat{\mathbf{r}} \cdot \mathbf{v}_{mnk}, \; \tilde{\imath}\hat{\boldsymbol{\theta}} \cdot \mathbf{v}_{mnk}, \; \hat{\boldsymbol{\phi}} \cdot \mathbf{v}_{mnk}] e^{\tilde{\imath}(m\phi)}, \tag{22}$$

which, comparing with (18)–(20), defines $\mathbf{v}_{mnk}$ as a real vector function of r and θ.

In the second problem, the viscous boundary layer correction for each inertial mode $\tilde{\mathbf{u}}_{mnk}$ is made to ensure that the tangential velocity vanishes at the bounding surface of the sphere. By virtue of the properties of a viscous boundary layer in rapidly rotating spheres, we can derive a fourth-order differential equation from (5) governing the boundary-layer flow on the bounding surface of the sphere

$$\left(\frac{\partial^2}{\partial \xi^2} - 4\tilde{\imath}\sigma_{mnk} \right)^2 \tilde{\mathbf{u}}_{mnk} + 4 (\hat{\mathbf{z}} \cdot \hat{\mathbf{r}})^2 \tilde{\mathbf{u}}_{mnk} = 0, \tag{23}$$

where ξ is a stretched boundary-layer variable $\xi = E^{-1/2} (1-r)$, which will be solved subject to the following four boundary conditions

$$(\tilde{\mathbf{u}}_{mnk})_{\xi=0} = -(\mathbf{u}_{mnk})_{r=1}, \tag{24}$$

$$\left(\frac{\partial^2 \tilde{\mathbf{u}}_{mnk}}{\partial \xi^2} \right)_{\xi=0} = -2 \left[\tilde{\imath}\sigma_{mnk} \mathbf{u}_{mnk} + (\hat{\mathbf{z}} \cdot \hat{\mathbf{r}})\hat{\mathbf{r}} \times \mathbf{u}_{mnk} \right]_{r=1}, \tag{25}$$

$$(\tilde{\mathbf{u}}_{mnk})_{\xi=\infty} = 0, \tag{26}$$

$$\left(\frac{\partial^2 \tilde{\mathbf{u}}_{mnk}}{\partial \xi^2} \right)_{\xi=\infty} = 0. \tag{27}$$

The fourth-order differential eq. (23) together with the four boundary conditions determines the solution of the spherical Ekman boundary layer. A straightforward but lengthy analysis gives rise to

$$\tilde{\mathbf{u}}_0 = -\sum_{mnk} A_{mnk} \tilde{\mathbf{u}}_{mnk}$$
$$= -\sum_{mnk} A_{mnk} \left[\mathcal{X}_{mnk} \exp\left(\beta_{mnk} E^{-1/2} \xi \right) \right.$$
$$\left. + \mathcal{Y}_{mnk} \exp\left(\gamma_{mnk} E^{-1/2} \xi \right) \right] e^{(\tilde{\imath}2\sigma_{mnk} - d_{mnk})t}, \tag{28}$$

where d_{mnk} is to be determined and

$$\beta_{mnk} = -\left(1 + \frac{\sigma_{mnk} + \cos\theta}{|\sigma_{mnk} + \cos\theta|} \tilde{\imath} \right) (\sigma_{mnk} + \cos\theta)^{1/2},$$

$$\gamma_{mnk} = -\left(1 + \frac{\sigma_{mnk} - \cos\theta}{|\sigma_{mnk} - \cos\theta|} \tilde{\imath} \right) (\sigma_{mnk} - \cos\theta)^{1/2},$$

and, $\mathcal{X}_{mnk}$ and $\mathcal{Y}_{mnk}$ are complex vectors defined as

$$\mathcal{X}_{mnk} = -\frac{1}{2} \left[\left(\hat{\boldsymbol{\theta}} \cdot \mathbf{v}_{mnk} + \hat{\boldsymbol{\phi}} \cdot \mathbf{v}_{mnk} \right)_{(r=1)} \left(\tilde{\imath}\hat{\boldsymbol{\theta}} + \hat{\boldsymbol{\phi}} \right) \right], \tag{29}$$

$$\mathcal{Y}_{mnk} = -\frac{1}{2} \left[\left(\hat{\boldsymbol{\theta}} \cdot \mathbf{v}_{mnk} - \hat{\boldsymbol{\phi}} \cdot \mathbf{v}_{mnk} \right)_{(r=1)} \left(\tilde{\imath}\hat{\boldsymbol{\theta}} - \hat{\boldsymbol{\phi}} \right) \right]. \tag{30}$$

It is anticipated that the critical latitudes, $\theta_c = \cos^{-1}(\sigma_{mnk})$, where the boundary layer solution breaks down, would not significantly affect the values of the asymptotic solution at an asymptotically small E, for example, (Greenspan 1968; Hollerbach & Kerswell 1995; Tilgner & Busse 2001).

Consider now the third problem in the asymptotic sequence which determines the viscous decay factors,

$$\tilde{\imath}2\sigma_{mnk}\mathbf{u}_{mnk1} + 2\hat{\mathbf{z}} \times \mathbf{u}_{mnk1} + \nabla p_{mnk1} = E\nabla^2 \mathbf{u}_{mnk}$$
$$- (\tilde{\imath}2\sigma_{mnk1} - d_{mnk}) \mathbf{u}_{mnk}, \tag{31}$$

$$\nabla \cdot \mathbf{u}_{mkn1} = 0, \tag{32}$$

where σ_{mnk1} represents the viscous correction to the inviscid half frequency σ_{mnk}. Partial differential eqs (31) and (32) represent an inhomogeneous boundary-value problem that requires a solvability condition. It is of significance to note that, when $E^{1/2}$ is not used as an expansion parameter, the term $E\nabla^2\mathbf{u}_{mnk}$ for the interior viscous dissipation not only must be retained but also can be dominant for non-spherical geometries as explained in Appendix A. With the results of the first and second problems in the asymptotic sequence, the viscous decay factor, d_{mnk}, a key element in the initial value problem, can be determined by the solvability requirement for the inhomogeneous eq. (31), which is

$$d_{mnk} = -\frac{1}{\int_V |\mathbf{u}_{mnk}|^2 \, dV} \text{Real} \left[\int_S p_{mnk}^* \hat{\mathbf{n}} \cdot \tilde{\mathbf{u}}_{mnk1} \, dS \right.$$
$$\left. + E \int_V \mathbf{u}_{mnk}^* \cdot \nabla^2 \mathbf{u}_{mnk} \, dV \right], \tag{33}$$

where $\hat{\mathbf{n}}$ is the normal vector of the container and p^*_{mkn} denotes the complex conjugate of the pressure p_{mnk}. While the expression (33) is generally valid, however, because of the intriguing and unique property in spherical geometry (Zhang *et al.* 2001),

$$\int_0^{2\pi}\int_0^{\pi}\int_0^1 \left(\mathbf{u}^*_{mnk}\cdot\nabla^2\mathbf{u}_{mnk}\right)r^2\sin\theta\,dr\,d\theta\,d\phi \equiv 0, \qquad (34)$$

for all values of m, n and k, the expression (33) becomes

$$d_{mnk}=\frac{\int_0^{2\pi}\int_0^{\pi}E^{1/2}\left[\int_0^{\infty}p^*_{mnk}\hat{\mathbf{r}}\cdot\nabla\times(\hat{\mathbf{r}}\times\tilde{\mathbf{u}}_{mnk})\,d\xi\right]\sin\theta\,d\theta\,d\phi}{\int_0^{2\pi}\int_0^{\pi}\int_0^1|\mathbf{u}_{mnk}|^2r^2\sin\theta\,dr\,d\theta\,d\phi}, \qquad (35)$$

where only the real part of the expression will be taken. With the explicit solution $\mathbf{u}_{mnk}$ given by (18)–(20), we can, after some manipulation, establish that

$$\int_0^{2\pi}\int_0^{\pi}\int_0^1|\mathbf{u}_{mnk}|^2r^2\sin\theta\,dr\,d\theta\,d\phi=\sum_{i=0}^{k}\sum_{j=0}^{k-i}\sum_{q=0}^{k}\sum_{l=0}^{k-q}$$

$$\times\frac{(-1)^{i+j+q+l}\pi(m+j+l-1)!}{2^{3-m}[2(m+i+j+q+l)+1]!!}\left[\frac{\sigma_{mnk}^{2(i+q)}}{(2i-1)!!}\right]$$

$$\times\left\{\frac{8iq(2i+2q-3)!!(m+j+l)}{\sigma_{mnk}^2}\right.$$

$$+\left[\frac{(m\sigma_{mnk}+m+2j\sigma_{mnk})(m\sigma_{mnk}+m+2l\sigma_{mnk})}{(1-\sigma_{mnk}^2)^2}\right.$$

$$+\left.\left.\frac{(m\sigma_{mnk}+m+2j)(m\sigma_{mnk}+m+2l)}{(1-\sigma_{mnk}^2)^2}\right](2i+2q-1)!!\right\}$$

$$\times\left[\frac{(1-\sigma_{mnk}^2)^{j+l}[2(m+k+i+j)-1]!!}{(2q-1)!!(k-i-j)!(k-q-l)!}\right]$$

$$\times\left[\frac{[2(m+k+q+l)-1]!!}{i!q!j!l!(j+m)!(m+l)!}\right]. \qquad (36)$$

Making use of the interior solution p_{mnk} and $\mathbf{u}_{mnk}$ given by (17)–(20) and the boundary layer solution $\tilde{\mathbf{u}}_{mnk}$ given by (28), each integral in the right-hand side of (35), though lengthy, can be derived and evaluated, yielding the values of the viscous decay factors d_{mnk} for all possible m, n, k. A general expression for the decay factors d_{mnk} of the equatorially symmetric inertial waves is
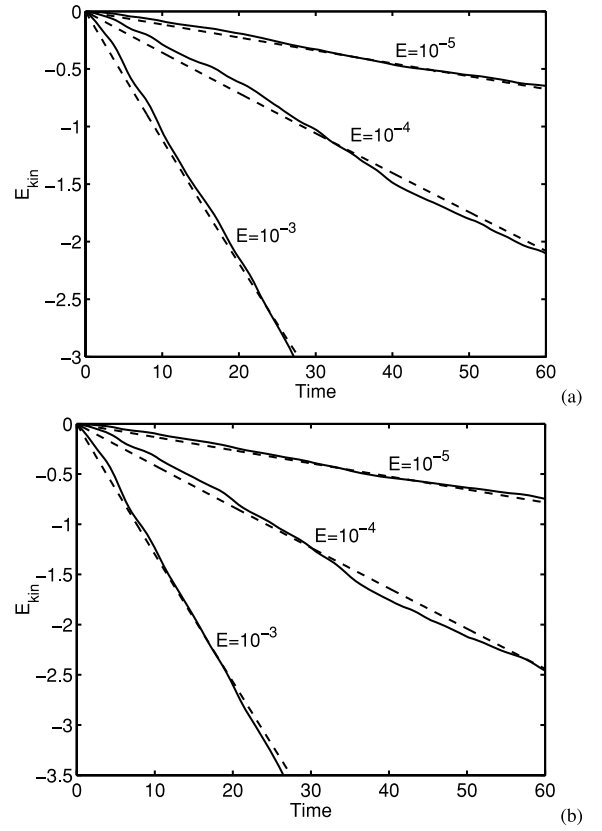
$$d_{mnk}=\frac{E^{1/2}\pi}{\int_0^{2\pi}\int_0^{\pi}\int_0^1|\mathbf{u}_{mnk}|^2r^2\sin\theta\,dr\,d\theta\,d\phi}$$

$$\times\int_0^{\pi}\left[\frac{(\sigma_{mnk}+\cos\theta)}{\sqrt{|\sigma_{mnk}+\cos\theta|^3}}\right]$$

$$\times\mathcal{P}_N(\theta)(\hat{\boldsymbol{\phi}}\cdot\mathbf{v}_{mnk}+\hat{\boldsymbol{\theta}}\cdot\mathbf{v}_{mnk})_{r=1})\,d\theta, \qquad (37)$$

where $\mathcal{P}_N$ is associated with the pressure at the outer spherical boundary

$$\mathcal{P}_N=\sum_{i=0}^{N}\sum_{j=0}^{N-i}C_{ijmN}\sigma_{mnk}^{2i}\left(1-\sigma_{mnk}^2\right)^j\sin^{m+2j}\theta\cos^{2i-1}\theta$$

$$\times\left[(m+2j)\cos^2\theta-2i\sin^2\theta-m\cos\theta\right].$$

It follows that the general time-dependent solution of the initial value problem can be written as

$$\mathbf{u}(\mathbf{x},t)=\sum_{mnk}\left(\frac{\int_V\mathbf{u}^*_{mnk}\cdot\mathbf{U}_0\,dV}{\int_V|\mathbf{u}_{mnk}|^2\,dV}\right)$$

$$\times\left[\mathbf{u}_{mnk}-\mathcal{X}_{mnk}\exp\left(\beta_{mnk}E^{-1/2}\xi\right)\right.$$

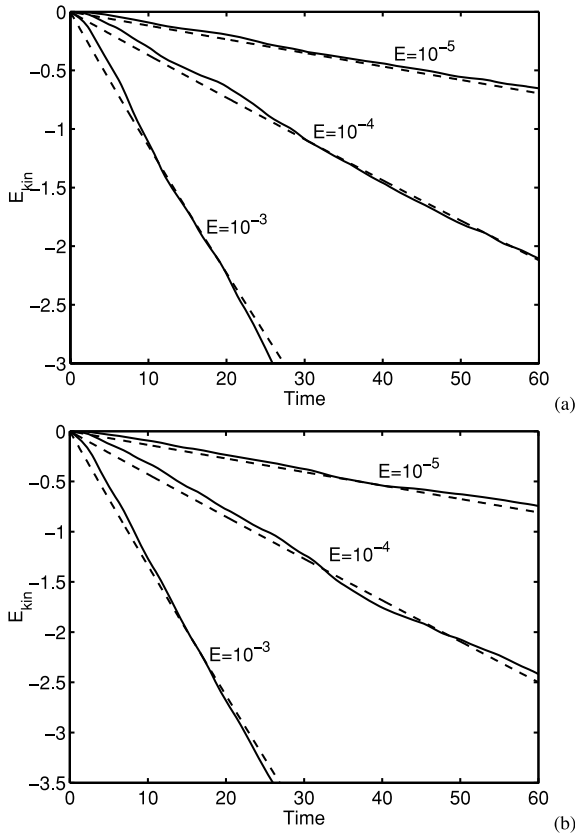$$\left.-\mathcal{Y}_{mnk}\exp\left(\gamma_{mnk}E^{-1/2}\xi\right)\right]e^{(i2\sigma_{mnk}-d_{mnk})t} \qquad (38)$$

Figure 1. Normalized kinetic energies, $E_{\text{kin}}(t)$, for solutions of the initial value problem, in the logarithmic scale, as a function of time with a toroidal initial velocity distribution (47) for three different values of E: (a) for the case for $M=2$, $L=M+1$ and (b) for $M=3$, $L=M+1$ in (47). Both asymptotic and numerical solutions with exactly the same initial condition and parameters are shown: the solid lines are for numerical simulations while the dashed lines for the corresponding asymptotic solutions.

for the ensuing transient motion of the problem. Four steps are required to compute an asymptotic time-dependent solution of the initial value problem for a given initial flow $\mathbf{U}_0$: (i) use (18)–(20) to carry out the integral $\int_V\mathbf{u}^*_{mnk}\cdot\mathbf{U}_0\,dV$; (ii) calculate all possible σ_{mnk} from eq. (21); (iii) for each inertial mode $\mathbf{u}_{mnk}$ and σ_{mnk}, use (37) to determine its decay factor d_{mnk} and (iv) finally, the substitution of $\mathbf{u}_{mkn}$ given by (18)–(20), $\mathcal{X}_{mnk}$ and $\mathcal{Y}_{mnk}$ given by (29) and (30) and d_{mnk} given by (37) into the asymptotic expression (38) yields the required asymptotic time-dependent solution. Several asymptotic solutions of the initial value problem computed from (38) at several small values of E for prescribed physically acceptable initial flows $\mathbf{U}_0$ are shown Figs 1 and 2, which will be discussed and validated by the fuller numerics of the problem at exactly the same parameters in the next section.

4 VALIDATION OF THE ASYMPTOTIC SOLUTION BY NUMERICAL SIMULATION

The primary purpose of our numerical analysis, which is valid for both large and small Ekman numbers, is to validate the asymptotic analysis that is valid only for $E\ll1$. In the numerical analysis, we expand the velocity $\mathbf{u}$ as a sum of poloidal (v) and toroidal (w) components by writing

$$\mathbf{u}=\nabla\times\nabla\times[\mathbf{r}v(r,\theta,\phi,t)]+\nabla\times[\mathbf{r}w(r,\theta,\phi,t)], \qquad (39)$$

Figure 2. Normalized kinetic energies, $E_{kin}(t)$, for solutions of the initial value problem, on a logarithmic scale, as a function of time with the poloidal initial velocity distribution (46) for three different values of E: (a) for the case with $L = M = 2$ and (b) for $L = M = 3$ in (46). Both asymptotic and numerical solutions with exactly the same initial condition are shown: the solid lines are for the numerical simulations while the dashed lines for the corresponding asymptotic solutions.

where **r** is the position vector. Obviously the condition $\nabla \cdot \mathbf{u} = 0$ is automatically satisfied. Applying $\mathbf{r} \cdot \nabla$ and $\mathbf{r} \cdot \nabla \times \nabla \times$ onto (5), we obtain the two independent non-dimensional scalar equations,

$$\left[\left(E\nabla^2 - \frac{\partial}{\partial t} \right) \mathcal{L} + 2\frac{\partial}{\partial \phi} \right] \nabla^2 v + 2\mathcal{Q}w = 0, \qquad (40)$$

$$\left[\left(E\nabla^2 - \frac{\partial}{\partial t} \right) \mathcal{L} + 2\frac{\partial}{\partial \phi} \right] w - 2\mathcal{Q}v = 0, \qquad (41)$$

where the differential operators $\mathcal{L}$ and $\mathcal{Q}$ are defined as

$$\mathcal{L} = -r^2 \nabla^2 + \frac{\partial}{\partial r} r^2 \frac{\partial}{\partial r},$$

$$\mathcal{Q} = \hat{\mathbf{z}} \cdot \nabla - \frac{1}{2} \left(\mathcal{L}\hat{\mathbf{z}} \cdot \nabla + \hat{\mathbf{z}} \cdot \nabla \mathcal{L} \right).$$

In terms of v and w, the non-slip boundary condition (7) becomes

$$v = \frac{\partial v}{\partial r} = w = 0 \quad \text{at} \ r = 1, \qquad (42)$$

subject to the initial condition

$$\mathbf{u} = \mathbf{U}_0(r, \theta, \phi, t = 0). \qquad (43)$$

Eqs (40) and (41) are then solved numerically by expanding the velocity potentials in terms of spherical harmonics $[P_l^m (\cos \theta) e^{im\phi}]$

and of radial functions that satisfy the no-slip boundary condition,

$$w(\mathbf{x}, t) = \sum_{lnm} w_{ln}(t) \, r^l \, (1 - r) \, T_n \, (2r - 1) \, P_l^m(\theta)e^{im\phi}, \qquad (44)$$

$$v(\mathbf{x}, t) = \sum_{lmn} v_{ln}(t) \, r^l \, (1 - r)^2 \, T_n \, (2r - 1) \, P_l^m(\theta)e^{im\phi}, \qquad (45)$$

where $T_n(x)$ denotes the standard Chebyshev function, $w_{lnm}(t)$ and $v_{lnm}(t)$ are time-dependent complex coefficients to be determined and spherical harmonics are normalized such that

$$\frac{1}{4\pi} \int_0^{2\pi} \int_0^\pi \left| P_l^m(\cos \theta)e^{im\phi} \right|^2 \sin \theta d\theta \ d\phi = 1.$$

Note that the factor r^l in the expansions (44) and (45) is required to remove the singularity at the origin $r = 0$. On substitution of (44) and (45) into (40) and (41) and application of the standard numerical procedure, we are able to derive a system of ordinary differential equations for $w_{lnm}(t)$ and $v_{lnm}(t)$ which can be integrated numerically starting from a given physically acceptable initial condition $\mathbf{U}_0$.

Though any distribution of the initial velocity can be used in our numerical simulation, we shall consider the following parametrized initial distributions: either the purely poloidal flow given by

$$\mathbf{U}_0 = \nabla \times \nabla \times \left[\mathbf{r} r^L (1 - r)^2 P_L^M(\cos \theta)e^{i(M\phi)} \right], \qquad (46)$$

where L and M are the parameters of the flow, or the purely toroidal flow given by

$$\mathbf{U}_0 = \nabla \times \left[\mathbf{r} r^L (1 - r)P_L^M(\cos \theta)e^{i(M\phi)} \right], \qquad (47)$$

which represents a physically acceptable flow satisfying both $\nabla \cdot \mathbf{U}_0 = 0$ and the non-slip boundary condition at the spherical bounding surface. The same initial condition is also used in calculating asymptotic solutions (38). We have also tried other different forms of the initial condition, all showing a broadly similar behaviour.

In describing solutions of the initial value problem, we introduce the normalized kinetic energy, E_{kin}, of the time-dependent solution,

$$E_{kin}(t) = \frac{\int_0^{2\pi} \int_0^1 \int_0^\pi |\mathbf{u}(r, \theta, \phi, t)|^2 \, r^2 \sin \theta \, d\theta \, dr \, d\phi}{\int_0^{2\pi} \int_0^1 \int_0^\pi |\mathbf{U}_0|^2 \, r^2 \sin \theta \, d\theta \, dr \, d\phi},$$
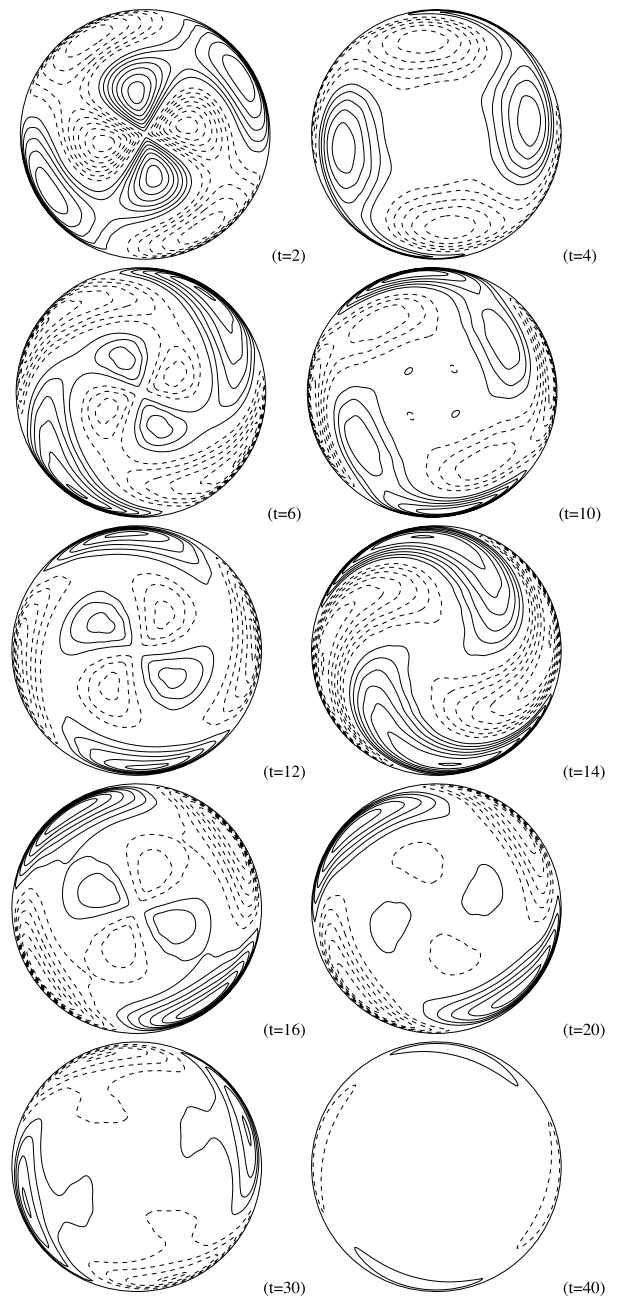
where **u** represents the time-dependent velocity calculated either from the numerical simulation of (40) and (41) or from the asymptotic solution (38). The normalized kinetic energies $E_{kin}(t)$ as a function of time for three different Ekman numbers, $E = 10^{-3}$, 10^{-4} and 10^{-5}, subject to exactly the same toroidal initial condition (47), are shown in Fig. 1 while similar solutions but subject to the poloidal initial condition (46) are displayed in Fig. 2. For the purpose of easy comparison, both asymptotic (dashed lines) and numerical (solid lines) solutions obtained with exactly the same initial condition are shown in Figs 1 and 2. Evidently, the asymptotic solution (38) of the initial value problem shows a satisfactory agreement with the numerical simulation, considering the numerical difficulties involved in accurately resolving the thin viscous boundary layer for $E \leq O(10^{-5})$. It is worth noting that, in calculating the kinetic energy E_{kin} for the asymptotic solution (38), the contribution from the viscous boundary flow is not included. This exclusion may be attributable to small but notable differences between the asymptotic solutions and numerical simulations.

It is also interesting to look at how the spatial structure of the initial flow varies with time, which is depicted in Fig. 3 calculated from the asymptotic solution (38) and in Fig. 4 calculated from the
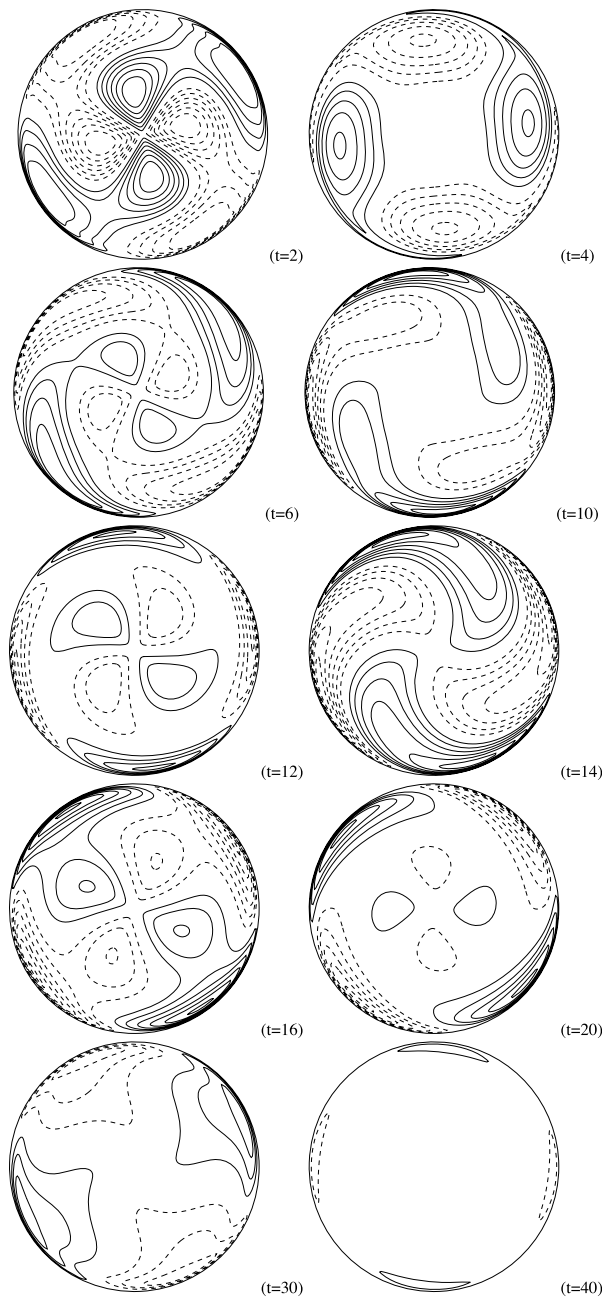
Figure 3. Contours of the azimuthal component of the flow, at the equatorial plane, of the asymptotic solution, starting from a toroidal initial velocity distribution (47) with $M = 2$, $L = M + 1$ for $E = 10^{-4}$ at ten different instants.

Figure 4. Contours of the azimuthal component, at the equatorial plane, of the numerical solution, starting from the toroidal initial velocity distribution (47) with $M = 2$, $L = M + 1$ for $E = 10^{-4}$ at 10 different instants. This numerical solution should be compared with the corresponding asymptotic solution shown in Fig. 3.

corresponding numerical simulation for the toroidal initial condition (47). There are several significant features emerging from the calculations. First, the agreement between the asymptotic and the fully numerical solution is remarkable over a long time interval, indicating the high accuracy of the asymptotic solution (38). Second, the spatial structure of the initial flow decays towards the rigid-body rotation in an oscillatory manner: it oscillates between the one- and two-layer structures. As a consequence of the controlling influence of rotation, the spatial-temporal variation of the initial value problem appears to be more complicated than we might anticipate. Finally, the type or form of the initial flow distribution does not alter the main characters of the problem. For example, three asymptotic

and numerical solutions starting with the poloidal initial flow (46) displayed in Fig. 2 show a broadly similar behaviour to that for the toroidal initial flow in Fig. 1. Moreover, an agreement between the asymptotic and fully numerical solutions for the poloidal initial flow (46) is also satisfactory.

5 GEOPHYSICAL APPLICATION

There are several reasons why the asymptotic time-dependent solution (38) is geophysically important and practically useful. Geophysically, it is well known that the extremely small value of the

Ekman number, a consequence of the Earth's rapid rotation and the small viscosity in the Earth's liquid core, causes severe difficulties in numerical modelling of core dynamics. Even with modern powerful supercomputers, modelling the core flow is usually restricted to the range of moderately small Ekman number $E \geq 10^{-5}$, which is still far from the geophysically realistic value, which is $E \leq 10^{-9}$ when the turbulent viscosity is used. Although the use of hyperviscosity in the modelling may remove these difficulties, its use alters the key dynamics of the fluid core in a fundamental and undesirable way (Zhang & Jones 1997). Understanding the core convection/dynamo at geophysically realistic E is yet to be achieved and remains a great challenge. Our analytical expression (38) is valid for an arbitrarily small Ekman number and, thus, can be employed to understand some aspects of the Earth's core dynamics for geophysically realistic E. Practically, our asymptotic expression (38) can be employed to describe the spatial and temporal variations of various time-dependent flows excited by any mechanism that is capable of producing an initial flow $\mathbf{U}_0$.

As a result of tidal torques from the Moon and Sun acting on the Earth's equatorial bulge, as well as mass transport in the atmosphere (Lambeck 1980) and the exchange of angular momentum between the solid mantle and fluid core (Dehant & Mathews 2007), the Earth's rotation axis changes its orientation with respect to the mantle on various timescales and the Earth is rotating non-uniformly. The effect of non-uniform rotation on the Earth's core flow determines how an original state of the flow is reconciled with a new orientation or a new speed of the Earth's rotation by adjusting its fluid motion to the new boundary condition (Roberts & Stewartson 1965). Suppose the Earth's mantle and the core fluid rotate together with a uniform angular velocity Ω_1 which is later changed suddenly to Ω_2. The bulk of the core fluid, away from the core–mantle interface, is initially unaffected and the thin viscous boundary layer at the core–mantle boundary rotates at a different speed compared to the bulk of the core fluid. As required by the conservation of mass, however, the interior core fluid will be sucked into this viscous boundary layer, leading to the new equilibrium over a long timescale. This complex process at an extremely small E, as an example, is accurately described by the asymptotic solution (38) of the initial value problem. It is also known that the problem of precessionally driven flows in the Earth's core can also be treated as an initial value problem (Roberts & Stewartson 1965). To illustrate a geophysical application of the asymptotic solution (38), we shall take an example in connection with the Earth's precessing flow. As an alternative cause of generating and maintaining the geomagnetic field (Bullard 1949; Malkus 1968), precessionally driven flows have been studied for a long time. As demonstrated by experimental studies (Malkus 1968; Vanyo *et al.* 1995), far away from the viscous boundary layer the weakly interior precessing flow is in the form of nearly solid-body rotation whose axis lies in the equatorial plane in the mantle frame of reference. The precessing flow may be approximately written as (Roberts & Stewartson 1965)

$$\mathbf{U}_0 = \nabla \times \left[\mathbf{r} \left(r \sin \theta \cos \phi \right) \left(1 - r \right) \right]. \tag{48}$$

Suppose that the axis of the Earth's rotation is moved impulsively; the core fluid motion approximately given by (48) would be produced (Roberts & Stewartson 1965). An interesting question is, then, in what manner, spatially and temporally, the fluid core will be reconciled with the new state of the Earth's rotation by adjusting its flow. The answer to this question may be provided by the asymptotic solution (38). It is important to note that, computationally, we can only reach moderately small Ekman numbers $E \geq 10^{-5}$. A numerical solution of this initial value problem computed at $E =$
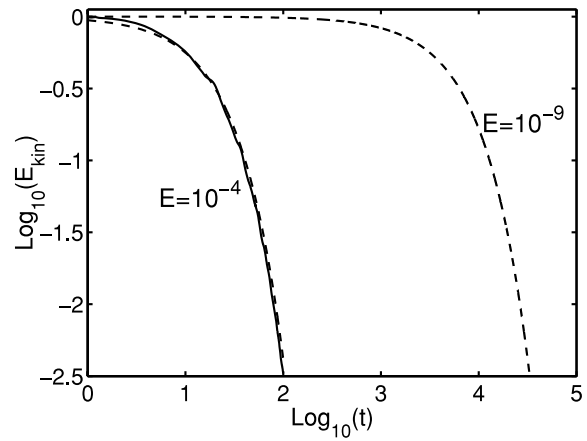
Figure 5. Normalized kinetic energies, $E_{\mathrm{kin}}(t)$, for solutions of the initial value problem, on a logarithmic scale, as a function of time starting with nearly rigid-body rotation (48) for two different values of E. Both asymptotic and numerical solutions with exactly the same initial condition are shown for $E = 10^{-4}$: the solid lines are the numerical simulations while the dashed lines are the corresponding asymptotic solutions. The asymptotic solution with the same initial condition is shown for $E = 10^{-9}$.

10^{-4}, along with the corresponding asymptotic solution, is shown in Fig. 5, showing a satisfactory quantitative agreement between the asymptotic solution and the corresponding numerical simulation. To extend the Ekman number E to the geophysically realistic value $E = 10^{-9}$, however, the numerical approach is no longer useful with today's computers and the asymptotic expression (38) has to be employed. The temporal dependence of the asymptotic solution obtained at $E = 10^{-9}$ is also displayed in Fig. 5. It reveals that the e-folding timescale of the flow is of order 10^2 yr, which is long enough to have influence on the magnetic field generation in the Earth's core. The spatial dependence of the flow is depicted in Fig. 6 by plotting contours of u_θ in the equatorial plane ($\theta = \pi/2$) at ten different instants. It is slightly surprising that the spatial structure of the flow undergoes, due to the controlling dominance of the Coriolis force at such a small E, complicated variations. This example illustrates how the asymptotic solution (38) can be used to describe the temporal and spatial variation of the core flow, excited by a sudden change of the Earth's rotation, at the geophysically realistic Ekman number $E = 10^{-9}$.

Another example of the initial value problem is related to the possible scenario for the maintenance and cessation of the Martian core dynamo proposed by Arkani-Hamed *et al.* (2008). They suggest that the tidal excitation of inertial waves by an asteroid drove and sustained the Martian core dynamo while the final impact of the asteroid on Mars might kill the Martian dynamo. Generally speaking, a giant impact on a planet would excite or initiate a significant perturbation, $\mathbf{U}_0$, in the planetary core that can modify the existing fluid motion and hence alter the existing dynamo process. A strong oscillatory flow, as shown in Fig. 3, resulting from the excitation of an external event, would yield a planetary magnetic signature. However, in order to elucidate the precise mechanism of how a giant impact affects the planetary dynamo process, one needs to establish a mathematical model between the giant impact and the initial perturbation $\mathbf{U}_0$ before making use of the asymptotic solution (38).

6 SUMMARY AND REMARKS

The spherical initial value problem is concerned with how an initial state of fluid motion in spherical geometry is damped by viscous
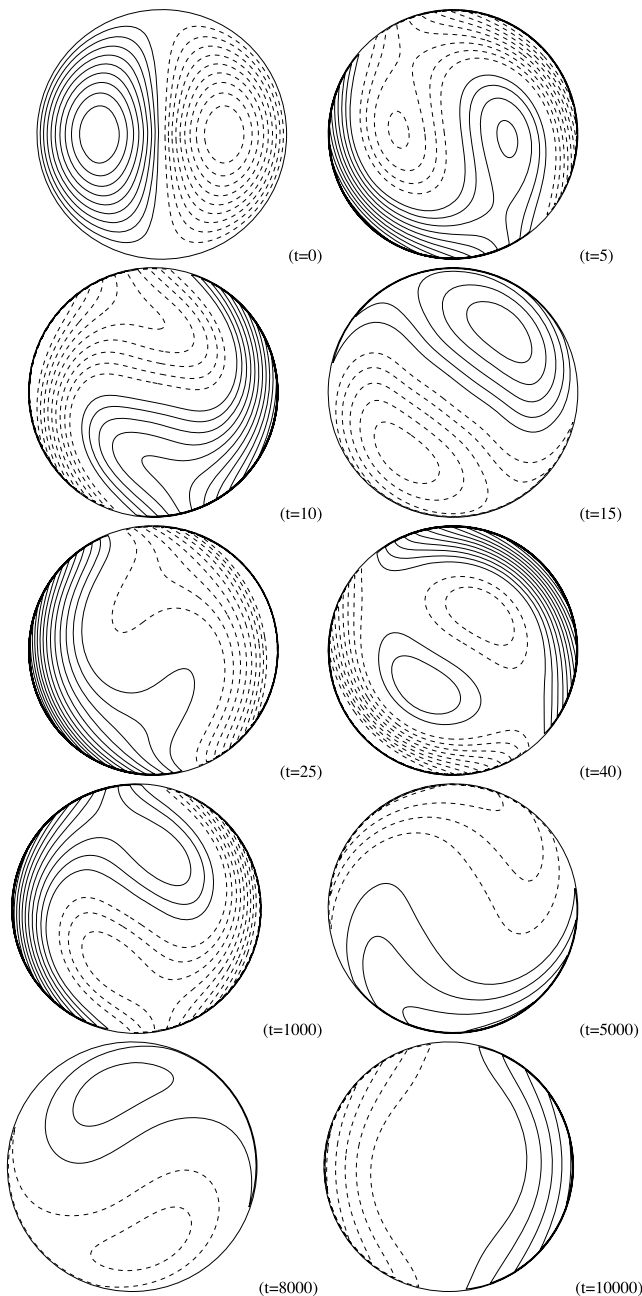
Figure 6. Contours of u_θ in the equatorial plane obtained from the time-dependent asymptotic solution (38) at $E = 10^{-9}$, starting from the initial velocity distribution (48) at ten different instants. Solid contours are for $u_\theta > 0$ while dashed contours are for $u_\theta < 0$.

dissipation and then decays towards a state of rigid-body rotation, representing an important classical geophysical and planetary physical problem. Its asymptotic solution contains three essential elements: interior inviscid inertial waves, the viscous boundary correction and the viscous decay factors for all possible inertial waves. We have obtained an explicit expression for time-dependent asymptotic solutions of the initial value problem in rapidly rotating spheres. We have also performed numerical simulations to compute time-dependent solutions of the initial value problem, showing a satisfactory quantitative agreement between the asymptotic and numerical analysis. This paper presents the first explicit time-dependent asymptotic solution and its numerical validation for the initial value

problem in rotating fluid spheres. It is also expected that the solution for a rotating sphere usually offers a good approximation to that for a rotating spherical shell with a small inner core (Zhang & Liao 2004).

Major magnetic planets, such as the Earth and Jupiter, share the same essential feature: they are rotating rapidly and the dynamics of their fluid cores is largely controlled by the Coriolis force. In other words, any dynamical problem of the fluid cores is characterized by an extremely small value of the Ekman number. This has resulted in severe difficulties in numerical simulation of the problem even with modern powerful supercomputers. Our asymptotic analysis reminds us of the fact that the asymptotic solutions like (38) in this paper, which is valid for an asymptotically small E, may represent the only way of reaching a physically realistic value of E in modelling planetary fluid cores.

Finally, in order to illustrate the mathematical consequence of the peculiar property of spherical inertial waves,

$$\int_V \mathbf{u}_{mnk}^* \cdot \nabla^2 \mathbf{u}_{mnk} \, dV \equiv 0, \tag{49}$$

and its fundamental difference between a sphere and other geometries, we shall briefly discuss both the asymptotic and numerical solution of the initial value problem in a rotating fluid channel, which is presented in Appendix A. The primary aim of Appendix A is to demonstrate a mathematically and physically non-trivial point: it is because of the peculiar property (49) for a sphere that the classical asymptotic expansion for the initial-value problem (Greenspan 1968) leads to a satisfactory quantitative agreement between the asymptotic and numerical solutions. As discussed in Appendix A, however, the asymptotic expansion based on $E^{1/2}$, for example, eqs (2.5.6) and (2.5.8) in Greenspan (1968), cannot lead to such a satisfactory quantitative agreement in non-spherical geometries for which (49) is no longer true.

ACKNOWLEDGMENTS

REFERENCES

Aldridge, K.D. & Lumb, L.I., 1987. Inertial waves identified in the Earth's fluid outer core, *Nature,* **325,** 421–423.

Arkani-Hamed, J., Seyed-Mahmoud, B., Aldridge, K.D. & Baker, R.E., 2008. Tidal excitation of elliptical instability in the Martian core: possible mechanism for generating the core dynamo, *J. geophys. Res.,* **113,** E06003, doi:10.1029/2007JE002982.

Aubert, J., Brito, D., Nataf, H.C., Cardin, P. & Masson, J.P., 2001. A systematic experimental study of rapidly rotating spherical convection in water and liquid gallium, *Phys. Earth planet Inter.,* **128,** 51–74.

Bullard, E.C., 1949. The magnetic flux within the earth, *Proc. R. Soc. A,* **197,** 433–453.

Davies-Jones, R.P. & Gilman, P.A., 1971. Convection in a rotating annulus uniformly heated from below, *J. Fluid Mech.,* **46,** 65–81.

Dehant, V. & Mathews, M.P., 2007. Earth rotation variations, in *Treatise of Geophysics* Vol. 3, pp. 295–349, eds Herring, T. & Schubert, G. Elsevier, Amsterdam.

Dormy, A.M., Soward, A.M., Jones, C.A., Jault, D. & Cardin, P., 2004. The onset of thermal convection in rotating spherical shells, *J. Fluid Mech.,* **501,** 43–70.

Greenspan, H.P., 1968, *The Theory of Rotating Fluids,* Cambridge University Press, Cambridge.

Hollerbach, R. & Kerswell, R.R., 1995. Oscillatory internal shear layers in rotating and precessing flows, *J. Fluid Mech.,* **298,** 327–339.

Holme, R., 1998. Electromagnetic core-mantle coupling-I. Explaining decadal changes in the length of day, *Geophys. J. Int.,* **132,** 167–180.

Holme, R. & de Viron, O., 2005. Geomagnetic jerks and a high-resolution length-of-day profile for core, *Geophys. J. Int.,* **160,** 435–439.

Jault, D., Gire, C. & Le Mouel, J.L., 1988. Westward drift, core motions and exchanges of angular momentum between core and mantle, *Nature,* **333,** 353–356.

Jones, C.A., Soward, A.M. & Mussa, A.I., 2000. The onset of thermal convection in a rapidly rotating sphere, *J. Fluid Mech.,* **405,** 157–179.

Kerswell, R.R., 1994. Tidal excitation of hydromagnetic waves and their damping in the Earth, *J. Fluid Mech.,* **274,** 219–241.

Kerr, R.A., 1994. Shoemaker-Levy dazzles, bewilders, *Science,* **265,** 601–602.

Lambeck, K., 1980, *The Earth's Variable Rotation: Geophysical Causes and Consequences,* Cambridge University Press, Cambridge.

Liao, X. & Zhang, K., 2008. On viscous decay factors for spherical inertial modes in rotating planetary fluid cores: comparison between asymptotic and numerical analysis, *Phys. Earth planet. Inter.,* **169,** 211–219.

Liao, X. & Zhang, K., 2009. Inertial oscillation, inertial wave and initial value problem in rotating annular channels, *Geophys. astrophys. Fluid Dyn.,* **103,** 199–222.

Malkus, W.V.R., 1968. Precession of the earth as the cause of geomagnetism, *Science,* **136,** 259–264.

Noir, J., Hemmerlin, F., Wicht, J., Baca, S.M. & Aurnou, J.M., 2008. Laboratory models of librationally-driven flow in planetary cores and sub-surface oceans. *Phys. Earth planet. Inter.,* **173,** 141–152.

Rieutord, M. & Valdettaro, L., 1997. Inertial waves in a rotating spherical shell, *J. Fluid Mech.,* **341,** 77–99.

Rieutord, M., Valdettaro, L. & Georgeot, B., 2002. Analysis of singular inertial modes in a spherical shell: the slender toroidal shell model, *J. Fluid Mech.,* **463,** 345–360.

Roberts, P.H. & Stewartson, K., 1965. On the motion of a liquid in a spheroidal cavity of a precessing rigid body: II, *Math. Proc. Cambridge Phil. Soc.,* **61,** 279–288.

Schmitt, D., 2006. Numerical study of viscous modes in a rotating spheroid, *J. Fluid Mech.,* **567,** 399–414.

Seyed-Mahmoud, B., Heikoop, J. & Seyed-Mahmoud, R., 2007. Inertial modes of a compressible fluid core model, *Geophys. Astrophys. Fluid Dyn.,* **101,** 489–505.

Tilgner, A. & Busse, F.H., 2001. Fluid flows in precessing spherical shells, *J. Fluid Mech.,* **426,** 387–396.

van Hoolst, T., Rambaux, N., Karatekin, Ö. & Baland, R.-M., 2009. The effect of gravitational and pressure torques on Titan's length-of-day variations, *Icarus,* **200,** 256–264.

Vanyo, J.P., Wilde, P., Cardin, P. & Olson, P., 1995. Experiments on precessing flows in the Earth's liquid core, *Geophys. J. Int.,* **121,** 136–142.

Zhang, K. & Jones, C.A., 1997. The effect of hyperviscosity On geodynamo models, *Geophys. Res. Lett.,* **24,** 2869–2872.

Zhang, K. & Liao, X., 2004. A new asymptotic method for the analysis of convection in a rapidly rotating sphere, *J. Fluid Mech.,* **518,** 319–346.

Zhang, K. & Liao, X., 2008. On the initial value problem in a rotating circular cylinder, *J. Fluid Mech.,* **610,** 425–443.

Zhang, K., Earnshaw, P., Liao, X. & Busse, F.H., 2001. On inertial waves in a rotating fluid sphere, *J. Fluid Mech.,* **437,** 103–119.

Zhang, K., Liao, X. & Earnshaw, P., 2004. The Poincare equation: a new polynomial and its unusual properties, *J. Math. Phys.,* **45,** 4777–4790.
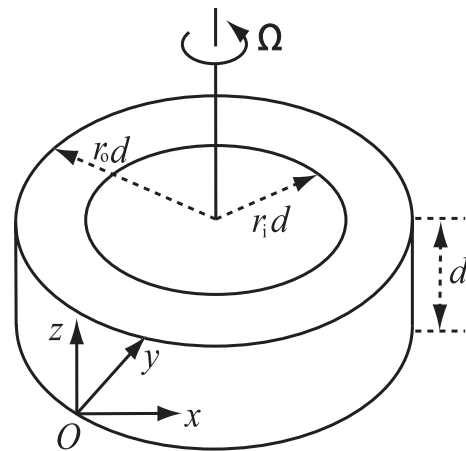
Figure A1. Geometry of a rotating annular channel with inner radius $r_i d$ and outer radius $r_o d$ whose fluid cavity is defined by $0 \leq y \leq \Gamma d$ and $0 \leq z \leq d$, where $\Gamma = r_o - r_i$ and x parallel to the sidewalls of the channel. The curvature effect is neglected by assuming $\Gamma / r_0 \ll 1$.

APPENDIX A: A SIMPLE EXAMPLE FOR COMPARISON: NON-AXISYMMETRIC SOLUTIONS OF THE INITIAL VALUE PROBLEM IN A ROTATING CHANNEL

A1 Introduction

Proposed first by Davies-Jones & Gilman (1971), a rotating narrow annular channel configuration (Fig. A1) is not only approximately realizable in laboratory experiments, more significantly in the present context, but also offers mathematical simplicity and clarity owing to the use of local cartesian coordinates. An analytical asymptotic solution of the initial value problem in channel geometry hence provides a unique opportunity to illustrate and give insight to the physics and basic mathematics of the problem and provide an interesting comparison with the spherical problem. Since the axisymmetric solution of the initial value problem in a rotating channel has been already studied (Liao & Zhang 2009), we shall briefly discuss slightly more complicated non-axisymmetric solutions of the problem in attempting to reveal why and how the spherical problem is both mathematically and physically unique.

A2 Asymptotic solution

We shall keep our discussion brief since the governing equations and the asymptotic approach/formulation for a channel are similar to that for a sphere. Consider a homogeneous fluid of kinematic viscosity ν and density ρ confined an annular channel, whose geometry is sketched in Fig. A1, of inner radius $r_i d$ and outer radius $r_o d$ with depth d, rotating uniformly about its vertical axis with a constant angular velocity Ω. The aspect ratio of the channel is denoted by $\Gamma = (r_o - r_i d)/d$. When the width of the channel (Γd) is much smaller than the outer radius $r_o d$, that is, $\Gamma / r_o \ll 1$, we can make a local approximation by neglecting the curvature effect of the annular channel (Davies-Jones & Gilman 1971), allowing the use of simple cartesian coordinates: azimuthal coordinate x, vertical coordinate given by z and inward radial coordinate y with the unit vectors ($\hat{\mathbf{i}}, \hat{\mathbf{j}}, \hat{\mathbf{k}}$).

Three essential analytical expressions in the asymptotic solution of the initial value problem—the inviscid inertial wave $\mathbf{u}_{mnk}$, the viscous boundary correction $\tilde{\mathbf{u}}_{mnk}$ and the viscous decay factor

d_{mnk}—can be readily derived for the channel. First, the inviscid inertial waves, solutions to (14) and (15) in a channel, can be written as

$$p_{mnk} = \left[\frac{(k\pi \sigma_{mnk})}{m\Gamma} \cos\left(\frac{k\pi y}{\Gamma}\right) + \sin\left(\frac{k\pi y}{\Gamma}\right) \right] \\ \times \cos(n\pi z)\, e^{\tilde{\imath}mx}, \tag{A1}$$

$$\hat{\mathbf{i}} \cdot \mathbf{u}_{mnk} = \frac{1}{2}\left[\frac{n^2\pi^2}{m\sigma_{mnk}} \sin\left(\frac{k\pi y}{\Gamma}\right) - \frac{k\pi}{\Gamma} \cos\left(\frac{k\pi y}{\Gamma}\right) \right] \\ \times \cos n\pi z\, e^{\tilde{\imath}mx}, \tag{A2}$$

$$\hat{\mathbf{j}} \cdot \mathbf{u}_{mnk} = \frac{\tilde{\imath}}{2}\left[\frac{(n^2\pi^2 + m^2)}{m} \sin\left(\frac{k\pi y}{\Gamma}\right) \right] \cos n\pi z\, e^{\tilde{\imath}mx}, \tag{A3}$$

$$\hat{\mathbf{k}} \cdot \mathbf{u}_{mnk} = -\frac{\tilde{\imath}}{2}\left[\frac{n\pi}{\sigma_{mnk}} \sin\left(\frac{k\pi y}{\Gamma}\right) + \frac{nk\pi^2}{\Gamma m} \cos\left(\frac{k\pi y}{\Gamma}\right) \right] \\ \times \sin n\pi z\, e^{\tilde{\imath}mx}, \tag{A4}$$

where the three indices (m, n, k) are related to the three spatial wavenumbers in the azimuthal, vertical and radial directions, respectively, $\mathbf{u}_{mnk}$ is arbitrarily normalized to keep the expression simple and the half-frequency σ_{mnk} is simply given by

$$\sigma_{mnk} = \pm \frac{n\pi}{\sqrt{n^2\pi^2 + m^2 + (k\pi/\Gamma)^2}}, \tag{A5}$$

which obviously satisfies the bound $0 < |\sigma_{mnk}| < 1$. The second element involves the four boundary layer solutions on the bottom ($\widetilde{\mathbf{u}}_{mnk}^1$), the top ($\widetilde{\mathbf{u}}_{mnk}^2$), the outer sidewall of the channel ($\widetilde{\mathbf{u}}_{mnk}^3$) and inner sidewall ($\widetilde{\mathbf{u}}_{mnk}^{04}$), which can be readily derived but the details will not presented here. Based on our modified asymptotic expansion (11), the solvability condition required for the inhomogeneous boundary-value problem (31) and (32) in a channel gives rise to the viscous decay factors d_{mnk}

$$d_{mnk} = E\left(\frac{n^2\pi^2}{\sigma_{mnk}^2}\right) \\ + \sqrt{E}\left\{ \frac{\Gamma m^2}{(a^2 + n^2\pi^2)\left[k^2\pi^2 + \Gamma^2(m^2 + n^2\pi^2)\right]} \right\} \\ \times \left\{ \frac{2\pi^2\sqrt{|\sigma_{mnk}|}}{\Gamma^2}\left[k^2 + \left(\frac{nk\pi}{m}\right)^2 \right] \right. \\ + \left[(1 + \sigma_{mnk})^{1/2} + (1 - \sigma_{mnk})^{1/2}\right](a^2 + n^2\pi^2) \\ \times \frac{\left[k^2\pi^2 + \Gamma^2(m^2 + 2n^2\pi^2)\right]}{m^2\Gamma} \\ + \left[(1 - \sigma_{mnk})^{1/2} - (1 + \sigma_{mnk})^{1/2}\right] \\ \left. \times \left[\frac{2\Gamma n^2\pi^2(n^2\pi^2 + m^2)}{m^2\sigma_{mnk}} \right] \right\} \tag{A6}$$

for non-axisymmetric inertial modes with $m > 0$, where we have made use of the integral

$$\int_V \mathbf{u}_{mnk}^* \cdot \nabla^2 \mathbf{u}_{mnk}\, dV = -(m^2 + n^2\pi^2) \\ \times \frac{n^2\pi^2\left[k^2\pi^2 + \Gamma^2(m^2 + n^2\pi^2)\right]}{8\Gamma\sigma_{mnk}^2 m^2} < 0. \tag{A7}$$

It follows that the non-axisymmetric asymptotic solution of the initial value problem in a rapidly rotating channel with $E \ll 1$ is

$$\mathbf{u}(\mathbf{x}, t) = \sum_{mnk} \left(\frac{\int_V \mathbf{u}_{mnk}^* \cdot \mathbf{U}_0\, dV}{\int_V \mathbf{u}_{mnk}^* \cdot \mathbf{u}_{mnk}\, dV} \right) \\ \times \left(\mathbf{u}_{mnk} + \sum_{j=1}^4 \widetilde{\mathbf{u}}_{mnk}^j \right) e^{(2\tilde{\imath}\sigma_{mnk}t - d_{mnk}t)}, \tag{A8}$$

in which d_{mnk} is given by (A6) and

$$\int_V \mathbf{u}_{mnk}^* \cdot \mathbf{u}_{mnk}\, dV \\ = \frac{(m^2 + n^2\pi^2)\left[k^2\pi^2 + \Gamma^2(m^2 + n^2\pi^2)\right]}{8\Gamma m^2}. \tag{A9}$$

The asymptotic solution of the initial value problem (A8) is valid for any physically acceptable $\mathbf{U}_0$ at an asymptotically small E.

A3 Numerical solution: comparison with the asymptotic solution

We also undertake a numerical analysis for the purpose of validating the accuracy of the asymptotic solution (A8). In the numerical analysis for the non-axisymmetric problem in a rotating annular channel, which is valid for any values of E, a convenient decomposition involves the two velocity potentials Φ and Ψ

$$\mathbf{u} = \nabla \times \{[\Phi(y, z, t)\hat{\mathbf{k}} + \Psi(y, z, t)\hat{\mathbf{j}}]e^{\tilde{\imath}mx}\}. \tag{A10}$$

Making use of this expression and applying $\hat{\mathbf{j}} \cdot \nabla\times$ and $\hat{\mathbf{k}} \cdot \nabla\times$ onto the momentum eq. (5), we can derive two partial differential equations

$$0 = \left[\frac{\partial}{\partial t} - \left(\frac{\partial^2}{\partial y^2} + \frac{\partial^2}{\partial z^2} - m^2 \right) \right] \\ \times \left[\frac{\partial^2\Phi}{\partial y \partial z} - E\left(\frac{\partial^2}{\partial z^2} - m^2 \right)\Psi \right] + \tilde{\imath}2m\frac{\partial\Phi}{\partial z}, \tag{A11}$$

$$0 = \left[\frac{\partial}{\partial t} - \left(\frac{\partial^2}{\partial y^2} + \frac{\partial^2}{\partial z^2} - m^2 \right) \right] \\ \times \left[\frac{\partial^2\Psi}{\partial y \partial z} - E\left(\frac{\partial^2}{\partial y^2} - m^2 \right)\Phi \right] - \tilde{\imath}2m\frac{\partial\Psi}{\partial z}. \tag{A12}$$

In terms of Ψ and Φ, the no-slip condition becomes

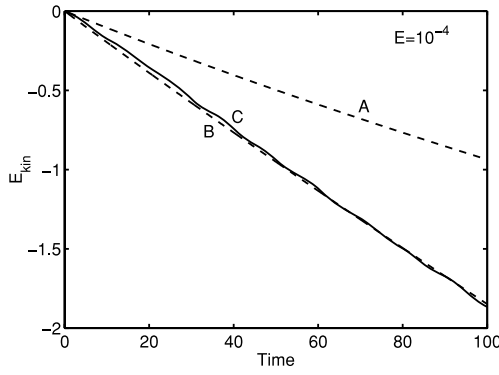$$\Psi = \Phi = \frac{\partial\Psi}{\partial z} = 0 \quad \text{at } z = 0, \ 1; \tag{A13}$$

$$\Psi = \Phi = \frac{\partial\Phi}{\partial y} = 0 \quad \text{at } y = 0, \ \Gamma. \tag{A14}$$

Eqs (A11) and (A12) are solved numerically by making the Galerkin-type expansion

$$\Phi = \sum_{l,k}^N \Phi_{kl}(t)\left[(1 - \hat{z}^2)\, T_l(\hat{z})\right]\left[(1 - \hat{y}^2)^2\, T_k(\hat{y})\right], \tag{A15}$$

$$\Psi = \sum_{l,k}^N \Psi_{kl}(t)\left[(1 - \hat{z}^2)^2\, T_l(\hat{z})\right]\left[(1 - \hat{y}^2)\, T_k(\hat{y})\right], \tag{A16}$$

where $\hat{y} = (2y/\Gamma - 1)$ and $\hat{z} = (2z - 1)$, which automatically satisfies the no-slip condition. Substitution of (A15)–(A16) into (A11)–(A12) results in a system of ordinary differential equations

Figure A2. Normalized kinetic energies, $E_{\text{kin}}(t)$, of the initial value problem are shown as a function of time at $E = 10^{-4}$ for $j_0 = n_0 = M = 2$ and $\Gamma = 2$ in (A17). Here (A) is obtained from the asymptotic solution using $E^{1/2}$ as the expansion parameter, (B) represents our asymptotic solution given by (A8) and (C) is from the corresponding numerical simulation.

for $\Psi_{kl}(t)$ and $\Phi_{kl}(t)$ which is integrated numerically starting from any given physically acceptable initial flow $\mathbf{U}_0$. For our numerical and asymptotic analysis, we choose the parametrized initial condition

$$\mathbf{U}_0(x, y, z, t = 0) = \left[\nabla \left(\Psi_0(y, z) e^{iMx} \right) \right] \times \hat{\mathbf{j}}, \tag{A17}$$

where $\Psi_0(y, z) = [(y/\Gamma)^2 \sin(j_0 \pi y/\Gamma)](1 - \hat{z}^2)^2 \cos(n_0 \pi z)$ with n_0 and j_0 being parameters. We have also tried different forms of the initial condition, all showing a broadly similar behaviour.

Fig. A2 shows three different time-dependent solutions of the initial value problem subject to exactly the same initial condition and parameters. In Fig. A2, line A represents the classical asymptotic solution taking $E^{1/2}$ as the expansion parameter (Greenspan 1968), line B denotes our asymptotic solution given by (A8) without taking $E^{1/2}$ as the expansion parameter, and line C is obtained from the fully numerical simulation. All our numerical integrations are performed up to $t = \mathrm{O}(E^{-1/2}) = 100$ for $E = 10^{-4}$. Evidently, our asymptotic solution (A8) gives a satisfactory agreement with the numerical simulation while the asymptotic solution taking $E^{1/2}$ as the expansion parameter (Greenspan 1968) does not.

Let's look at why the classical asymptotic solution taking $E^{1/2}$ as the expansion parameter cannot lead to a satisfactory agreement. At the root of the difference between cases A and B in Fig. A2 is the effect of the spatial-temporal non-uniformities. It is reflected by the relative importance between the interior contribution [E-term in (A6)], which must be neglected in the formulation taking $E^{1/2}$ as the expansion parameter, see page 42, Section 2.5 (Greenspan
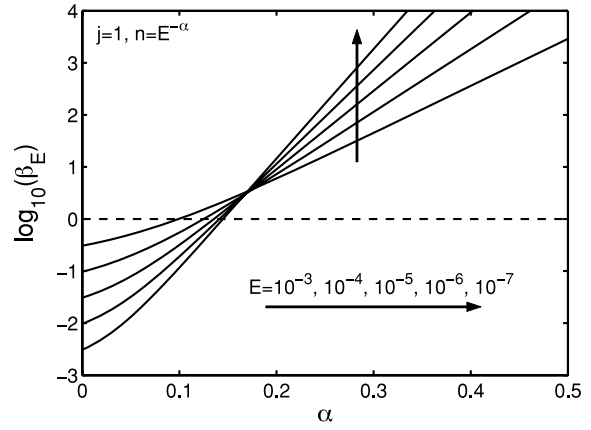
Figure A3. The ratio, β_E, of the E-term to the $E^{1/2}$-term in (A6) for $\Gamma = 2$, $j = 1$, $m = 2$ and $n = E^{-\alpha}$ is shown as a function of α for five different values of E. Note that $\beta_E \geq \mathrm{O}(1)$ when the wavenumber $n \geq \mathrm{O}(E^{1/6})$ for any sufficiently small E.

1968)], and the boundary-layer contribution [$E^{1/2}$-term in (A6)]. The ratio of the interior to boundary-layer contributions is given by

$$\beta_E = \left| \frac{E \int_V \mathbf{u}_{mnk}^* \cdot \nabla^2 \mathbf{u}_{mnk} \, dV}{\int_S p_{mnk}^* \hat{\mathbf{n}} \cdot \tilde{\mathbf{u}}_{mnk1} \, dS} \right|$$
$$= \frac{E\text{-term in } (A6)}{E^{1/2}\text{-term in } (A6)} \geq \mathrm{O}(1) \quad \text{as} \quad E \to 0, \tag{A18}$$

when $n \geq \mathrm{O}(E^{-1/6})$ for any sufficiently small E. Fig. A3 shows $\log_{10}[\beta_E]$ as a function of α ($n = E^{-\alpha}$) for five different values of E with $m = 2$, indicating that the E-term in (A6) that is completely neglected in the classical asymptotic formulation by taking $E^{1/2}$ as the expansion parameter (Greenspan 1968) is actually dominant when $n \geq \mathrm{O}(E^{-1/6})$. This indicates, generally speaking, that the spatial and temporal non-uniformities of the initial value problem prevent us from formulating the correct form of the asymptotic expansion on the basis of $E^{1/2}$. However, the problem in a sphere represents an unusual exception because

$$E \int_V \mathbf{u}_{mnk}^* \cdot \nabla^2 \mathbf{u}_{mnk} dV \equiv \mathbf{0},$$

which should be contrasted to the corresponding (A7) for a channel. This fundamental difference between a sphere and a channel may be attributable to the fact that spherical inertial waves are in the form of double polynomials while channel inertial waves are represented by trigonometric functions.